nature genetics

# Dampening of expression oscillations by synchronous regulation of a microRNA and its target

Dong hyun Kim[1,2,4], Dominic Grün[3] & Alexander van Oudenaarden[1–3]

**The complexity of multicellular organisms requires precise spatiotemporal regulation of gene expression during development. We find that in the nematode *Caenorhabditis elegans* approximately 2,000 transcripts undergo expression oscillations synchronized with larval transitions while thousands of genes are expressed in temporal gradients, similar to known timing regulators. By counting transcripts in individual worms, we show that pulsatile expression of the microRNA (miRNA) *lin-4* maintains the temporal gradient of its target *lin-14* by dampening its expression oscillations. Our results demonstrate that this insulation is optimal when pulsatile expression of the miRNA and its target is synchronous. We propose that such a miRNA-mediated incoherent feed-forward loop is a potent filter that prevents the propagation of potentially deleterious fluctuations in gene expression during the development of an organism.**



Proper development of a multicellular organism relies on the faithful expression of developmental genes. However, gene expression dynamics in any individual cell are inevitably noisy, owing to stochastic molecular events[1] and global intracellular fluctuations in cellular components due to environmental perturbation[2]. Such fluctuations, when inappropriately controlled, could be detrimental, as they could potentially interfere with the proper expression of important developmental genes and could create uncertainty in developmental outcomes. Unexpectedly, developmental phenotypes of multicellular organisms under normal conditions are robustly reproduced, suggesting that these animals successfully dampen undesired fluctuations in the expression of genes that require precise control. However, these control mechanisms are largely unexplored.

Larval development of the nematode *C. elegans* is an excellent model system for investigating mechanisms that control developmental gene expression because its physiological state changes almost discretely during four successive larval stages (L1–L4). These changes are mediated by both rhythmically and temporally graded expression of key developmental genes in the same cell or tissue that are known to be required for normal progression of developmental events[3–5]. At the end of each larval stage, the worm passes through a quiescent, sleep-like behavioral state, lethargus[6], which is followed by a molt[7]. In the hypoderm, collagen-encoding molting and nuclear hormone receptor genes exhibit periodic expression that peaks once every larval stage, potentially acting as timers for the molting cycle[4,5]. Although most somatic tissues are already differentiated upon hatching, the body plan of the worm is further finalized by expansion and migration of hypodermal, intestinal and neuronal tissues[8]. The germ line maturates, and the worm becomes reproductively competent[9]. In contrast to events in the molting cycle, many of these developmental events have timing that is often precisely controlled by cell fate regulators expressed in a temporal gradient in which the level of these regulators monotonically decreases as development progresses[10–12]. Mutations of these so-called heterochronic genes lead to precocious or retarded development (omission or reiteration of developmental events, respectively)[10,11,13,14].

The transcription factor *lin-14* was among the first heterochronic genes described in *C. elegans*[3,13] and is a target of the miRNA lin-4 (ref. 15). miRNAs are ~22-nucleotide noncoding RNAs that guide a multiprotein complex to its complementary elements in the 3′ UTR of protein-coding genes and repress protein production by translational inhibition or transcript degradation[16]. Gene products of *lin-14* trigger dosage-dependent, larval stage–specific programs[10]. Downregulation of the LIN-14 protein by *lin-4* was found to be critical for the transition from L1- to L2-specific programs, and further downregulation at the end of L2 is required for the transition to L3-specific programs. When *lin-4*–mediated repression is lost, LIN-14 protein levels remain high, and worms display a 'retarded' phenotype where cells variably reiterate early developmental programs[17]. The importance of gradually decreasing *lin-14* expression was first inferred from genetic analyses[10], which suggested that cells in wild-type worms can distinguish distinct levels of the activities encoded by these genes at specific times during the first two larval stages. Despite the fact that *lin-4* and *lin-14* are historically the first miRNA and target genes, respectively, to be discovered and have been extensively studied, mechanisms that control the integrity of the temporal gradient have not been elucidated.

In our study, we used next-generation mRNA sequencing to explore the dynamics of the *C. elegans* larval transcriptome with unprecedented temporal resolution to systematically determine the extent to

[1]Department of Physics, Massachusetts Institute of Technology, Cambridge, Massachusetts, USA. [2]Department of Biology, Massachusetts Institute of Technology, Cambridge, Massachusetts, USA. [3]Hubrecht Institute, Royal Netherlands Academy of Arts and Sciences and University Medical Center Utrecht, Utrecht, The Netherlands. [4]Present address: Samsung Fire & Marine Insurance Co., Ltd., Seoul, Republic of Korea. Correspondence should be addressed to A.v.O. (a.vanoudenaarden@hubrecht.eu).

Received 25 January; accepted 22 August; published online 15 September 2013; doi:10.1038/ng.2763

which gene expression fluctuates during development. On the basis of these data, we classify genes into groups that either exhibit periodic expression synchronized with the molting cycle or display a temporal gradient, similar to that of heterochronic genes. Using computational analyses, we assess the role of miRNAs in regulating these different expression patterns. We then performed a detailed characterization of the expression dynamics of miRNA *lin-4* and its target *lin-14* and propose a new regulatory role for miRNA in which it acts as a damper on oscillations in the expression of target genes. Our findings suggest that, during *C. elegans* postembryonic development, expression of *lin-14* is driven by an upstream regulator that oscillates in phase with the molting cycle. The transcript levels of *lin-14*, however, do not oscillate in wild-type worms owing to synchronous oscillatory expression of *lin-4*. This gene network motif is identical to an incoherent feed-forward motif[18]. Our mathematical model analysis suggests that this miRNA-mediated incoherent feed-forward circuit is crucial for efficient dampening of oscillations in the expression of the miRNA target, ensuring a stable temporal gradient of *lin-14*.

## RESULTS

### Thousands of genes display periodic expression in synchrony with the molting cycle

To determine the precise dynamics of the *C. elegans* transcriptome during larval development, we conducted RNA sequencing (RNA-seq) experiments using polyadenylated RNA libraries prepared from synchronized larval populations representing 20 different developmental time points, ranging from 0 h to 38 h after hatching with 2-h resolution, at 20 °C (**Fig. 1a**). This timeframe spans the first three larval stages (L1, L2 and L3). In an independent experiment, we prepared and sequenced libraries for the L4 stage, again with 2-h resolution, ranging from 38 h to 48 h after hatching. We used the Illumina HiSeq 2000 platform to generate single-end 40-bp reads. Reads were mapped to recently published improved gene models[19], and expression was aggregated across all isoforms derived from a given gene locus. In our analysis, we discarded genes that had an average RPKM (reads per kilobase of exon model per million mapped reads) value[20] of less than 1 and detected 16,776 reliably expressed annotated gene loci. We first examined how transcriptome-wide gene expression levels varied by computing pairwise correlations between transcriptomes at different developmental time points (**Supplementary Fig. 1a**). Interestingly, we found that pairwise correlations did not monotonically decrease when comparing more distant time points. For example, the correlation coefficient for comparison of expression levels at 10 h and 16 h was smaller than when comparing expression at 10 h and 22 h (**Supplementary Fig. 1a**). To test whether the absence of monotonic temporal decrease of pairwise correlation was a robust phenomenon, we cultured synchronized larval populations at 25 °C. At this elevated temperature, worms develop normally but at an accelerated rate. We therefore isolated polyadenylated RNA libraries every 1.5 h and found strikingly similar pairwise correlations to those obtained at 20 °C (**Supplementary Fig. 1a**). This finding suggested that the *C. elegans* transcriptome is modulated periodically during larval development.

To detect periodic signals from the expression profiles of individual genes, we first decomposed the temporal expression profile of each gene into a trend and a cycling component using Hodrick-Prescott filtering. Next, we assessed the significance of autocorrelation of the cycling component. Genes with a significant autocorrelation (Durbin-Watson $P < 0.05$) were classified as cycling genes, whereas all other genes were termed graded, as changes in their temporal expression were dominated by the slowly changing trend component. We resolved distinct modes of expression within the groups of cycling and graded genes and reduced the entire 16,776 profiles to reproducible clusters of gene expression profiles (Online Methods, **Supplementary Fig. 1b** and **Supplementary Table 1**). Although the majority of genes exhibited graded expression patterns (14,703 genes; 88%), we were surprised to find a large number of genes with cycling expression (2,073 genes; 12%). In total, 12,695 graded genes (86%) and 1,592 cycling genes (77%) were assigned to robust clusters. For an example, we considered the cuticle collagen gene *dpy-10*, which displays periodic expression[7]. This gene cycled with a period length of about 12 h and peaked once every larval stage (**Fig. 1b**). A 30-fold change was observed between expression minima and maxima, and these pronounced expression changes occurred within 6 h. All 231 genes that coclustered with *dpy-10* are shown in **Figure 1b**. We observed similar behavior for this group of genes at 25 °C, although the period length was shorter owing to accelerated development (**Fig. 1c**). We found that, after we accounted for a homogenous ~30% increase in the speed of development at 25 °C, genome-wide temporal gene expression profiles were indeed highly similar to those for independently grown worm populations at 20 °C (**Supplementary Fig. 2**).

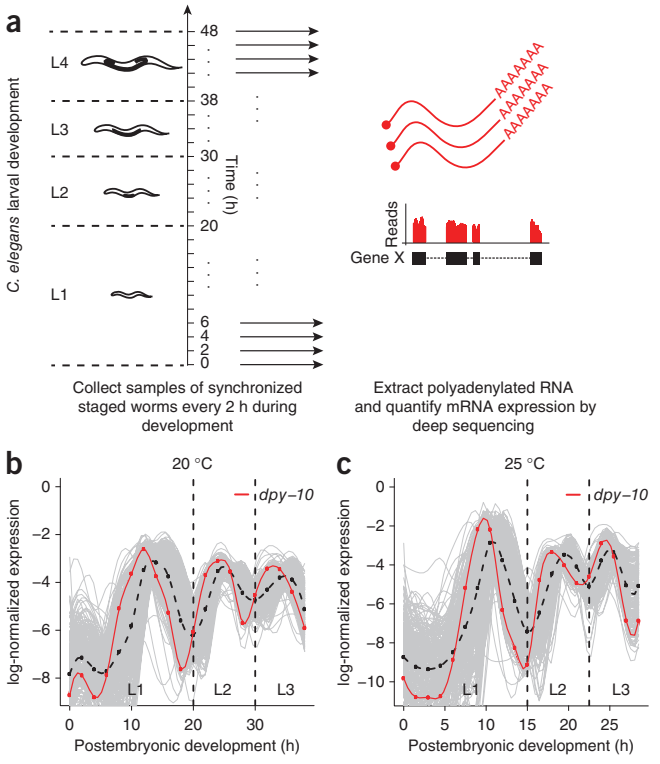


**Figure 1** A number of genes display cycling expression dynamics synchronous with the molting cycle during larval development. (**a**) Experimental design. After synchronizing hatched worms by starvation, we collected samples every 2 h (1.5 h) during larval development at 20 °C (25 °C). For each sample, transcript expression was measured by sequencing of polyadenylated RNA. (**b**,**c**) Normalized expression profiles of all 231 genes (gray) that cocluster with the collagen-encoding molting gene *dpy-10* (red) known to exhibit periodic expression[7]. Cycling expression was observed at 20 °C (**b**) and 25 °C (**c**). The average profile is indicated by the dashed black curves. All curves are spline fits of discrete expression profiles (red dots for *dpy-10*). Dashed lines separate larval stages.

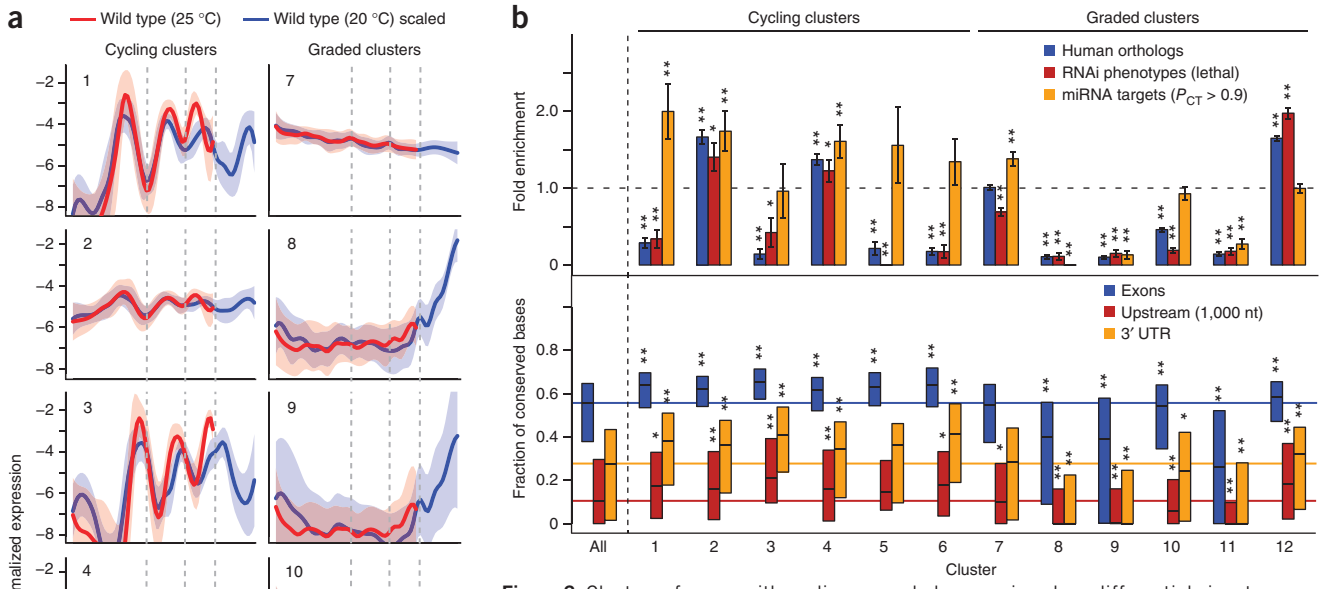


**Figure 2** Clusters of genes with cycling or graded expression show differential signature of post-transcriptional regulation. (**a**) Average normalized expression profiles of distinct expression clusters (**Supplementary Table 1**) for cycling genes and graded genes at 20 °C and 25 °C. Shading indicates s.d. For developmental times longer than 38 h at 20 °C, data from an independently grown worm population were used. Developmental time at 25 °C was rescaled linearly by a factor of 0.77 to account for faster development and to make expression at different temperatures comparable (**Supplementary Fig. 2**). Dashed gray lines indicate transitions between larval stages at 20 °C. The cluster number is indicated in the upper left corner. (**b**) Top, enrichment of human orthologs as a proxy for gene age, of lethal RNAi phenotypes to measure the fraction of genes essential for survival and of predicted conserved miRNA targets to estimate the extent of post-transcriptional regulation for each cluster. Error bars are based on random counting statistics. *P* values were computed by Fisher's exact test. Data are shown for all clusters individually and in total. Bottom, percentage of conserved nucleotides within aligned contigs of total exonic sequence, of 3′ UTR sequence and of 1 kb of upstream sequence. Conservation was measured using multiple-sequence alignments of *C. elegans*, *C. briggsae* and *C. remanei*, downloaded from the UCSC Genome Browser[27]. Unaligned sequence of *C. elegans* was counted as mismatches to obtain a conservative estimate. Shown are the interquartile range (box) and the median (black bar). Data are shown for all clusters individually and in total. Colored lines indicate medians across all genes. *P* values were computed by two-sided *t* tests. $*P < 0.05$; $**P < 0.001$.



## Cycling genes have a distinctive functional signature and are highly enriched in putative miRNA targets

Among the robust gene expression clusters identified, we found six distinct clusters of coexpressed cycling genes (**Fig. 2a**). Notably, average expression profiles for all of these clusters displayed a period length of approximately 12 h and appeared to be synchronized with larval transitions. Four clusters (clusters 1, 3, 5 and 6) cycled with similar amplitudes but small relative shifts in the expression peaks. The two remaining clusters (clusters 2 and 4) displayed less pronounced expression peaks, and the average profiles of these clusters were phase shifted by half a period length. Graded gene expression profiles were distributed among six robust clusters with decreasing (clusters 7, 10 and 11), increasing (clusters 8 and 9) or constant (cluster 12) temporal expression. Notably, robust clusters of coregulated genes with pronounced pulsatile but non-cycling expression were not found.

To investigate and characterize coexpressed genes, we first computed functional enrichments in Gene Ontology (GO) terms for each of the clusters (Online Methods and **Supplementary Table 2**). A summarized annotation is given in **Table 1**. Not unexpectedly, cycling clusters with pronounced amplitudes (clusters 1, 3 and 6) were associated with molting, a process that occurs at the end of each larval stage, during which the worm replaces its entire exoskeleton by proteolysis of old cuticle and generation of new cuticle[7]. Other cycling clusters, however, were also preferentially associated with metabolic functions (cluster 4) and germline development (cluster 2). Hence, cycling genes are not only associated with molting but appear to exert more diverse functions.

Within the graded clusters, genes with temporally decreasing expression (clusters 7, 10 and 11) were enriched in annotations related to sensory perception and nervous system development and, more generally, were associated with transcription and signaling. Enrichment of these categories of genes probably reflects ongoing neuronal differentiation during the first two larval stages. An increased number of genes with maximal expression toward the end of larval development (clusters 8 and 9) appears to be involved in (de)phosphorylation and gamete generation. These genes most likely become expressed in the germ line upon onset of spermatogenesis during the fourth larval stage[9]. Interestingly, a pronounced overrepresentation of developmental gene annotations was observed for the largest cluster (cluster 12) with constant temporal expression. Presumably, many of these genes are switched on upon specification of somatic tissues during embryonic development and maintain tissue-specific expression during larval development and adulthood.

**Table 1 Summary of functional annotations of the expression clusters based on GO term enrichment analysis**

| Cluster | Number of genes | Summarized enriched biological processes ($P < 1 \times 10^{-5}$) |
|---|---|---|
| 1 | 231 | Molting cycle |
| 2 | 384 | Gonad morphogenesis, protein localization |
| 3 | 116 | Proteolysis |
| 4 | 544 | Metabolism |
| 5 | 92 | – |
| 6 | 225 | Cuticle development, proteolysis, body morphogenesis |
| 7 | 3,175 | Signaling, metabolism, transcription, nervous system development |
| 8 | 610 | (De)phosphorylation, gamete generation |
| 9 | 841 | (De)phosphorylation, gamete generation |
| 10 | 2,092 | Signaling, neurological system process, sensory perception, transcription |
| 11 | 932 | Sensory perception, transcription |
| 12 | 5,045 | Embryo development, larval development, reproduction, cell cycle |

For a full list of enriched GO terms, see **Supplementary Table 2**.

To analyze the essentiality of genes with distinct temporal expression patterns in the development and survival of the organism, we measured enrichment for lethal RNA interference (RNAi) phenotypes[21] (**Fig. 2b**). Consistent with the pronounced over-representation of developmental genes, the strongest enrichment was observed for cluster 12. Interestingly, the only other clusters (clusters 2 and 4) with an over-representation of lethal phenotypes belonged to the class of cycling genes. We observed a strikingly similar enrichment pattern for the fraction of genes with human orthologs (Online Methods), confirming the assumption that essential genes are preferentially evolutionarily old.

One of our major goals was to investigate the role of post-transcriptional regulation in modulating temporal gene expression patterns. We therefore screened the 3′ UTRs of all genes in a given expression cluster for the presence of conserved miRNA target sites. We used target predictions from TargetScanS[22] after discarding weakly conserved sites ($P_{CT} < 0.9$). Whereas three of the cycling clusters (clusters 1, 2 and 4) were significantly enriched in conserved miRNA targets, only one of the graded clusters (cluster 7) was enriched in these targets, and three graded clusters (clusters 8, 9 and 11) were strongly depleted of miRNA target sites. This observation suggests that post-transcriptional gene regulation could be required to mediate highly dynamic expression changes, which would be consistent with a more sensitive expression response upon the increased transcript degradation triggered by miRNAs[23–26]. Consistently, all but one of the cycling clusters exhibited, on average, significantly increased 3′ UTR sequence conservation (**Fig. 2b**), measured on the basis of multiple alignments to the related nematode species *Caenorhabditis briggsae* and *Caenorhabditis remanei*[27] ($P < 0.001$). We also detected overall enhanced sequence conservation of exonic sequence (coding exons and UTRs) and promoter sequence (annotated as 1 kb upstream of the transcription start site) for the cycling clusters (**Fig. 2b**). In contrast, conservation in the majority of the graded clusters (clusters 8–11) was significantly reduced (**Fig. 2b**). Although cycling genes were more highly conserved overall than graded genes, the difference in conservation was particularly pronounced for promoter and 3′ UTR sequence, where average conservation was low. Considering the under-representation of essential genes in most of the cycling clusters, it was unexpected to observe enhanced conservation of regulatory sequence. These findings, which are contradictory at first glance, could potentially be reconciled by a requirement for cycling genes to host a higher density of regulatory elements within promoters and 3′ UTRs to confer highly dynamic regulation.

## Temporal expression of lin-4 targets suggests specific role of lin-4 in maintaining temporal gradients

We identified miRNAs with preferences for predicted target genes with either cycling or graded expression (**Fig. 3a**,**b**). For instance, targets of miR-230 were strongly over-represented in two cycling clusters (clusters 1 and 6), and targets of miR-71 were enriched overall in cycling genes (**Fig. 3a**). Interestingly, miR-71 is necessary for larval survival after stress conditions[28] and promotes longevity[29,30]. Other miRNAs, such as the miR-1 family, had significantly increased numbers of targets in cycling and graded clusters (**Fig. 3a**).

In contrast, many predicted targets of the heterochronic miRNAs let-7 and lin-4 as well as many targets of the miR-51 family, one of the few miRNA families that is indispensible during embryonic development[31], were found among genes with a temporal expression gradient (**Fig. 3b**). The specificity of temporal gene expression profiles was particularly pronounced for lin-4 targets, which were highly concentrated in cluster 7. This observation suggests a major role for lin-4 in maintaining robust temporal gradients of its targets. Among these targets is the important developmental timing regulator *lin-14*, a classic heterochronic gene that has negatively graded temporal expression[3,10,13].

## The miRNA lin-4 shows periodic expression in synchrony with the molting cycle

To study whether lin-4 has any role in insulating *lin-14* from periodic fluctuations, we first measured mature lin-4 miRNA levels in total RNA extracts isolated from staged larvae using a quantitative RT-PCR

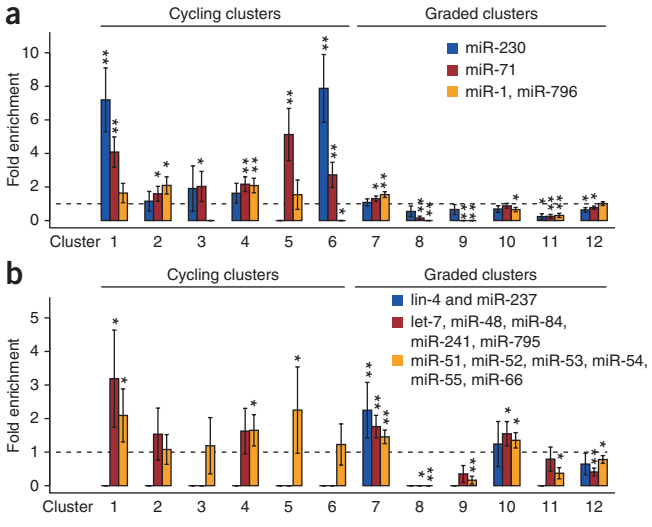


**Figure 3** Predicted targets of many miRNAs are enriched in temporally coexpressed genes. (**a**) Fold enrichment of predicted miRNA targets in cycling expression clusters. Targets of miR-230 are strongly over-represented in cycling clusters with pronounced amplitudes, whereas miR-1 and miR-796 targets are enriched in cycling clusters with low amplitudes. In contrast, predicted miR-71 targets are enriched in all cycling clusters. (**b**) Fold enrichment of predicted targets of developmental miRNAs. Targets are either dispersed across different expression clusters (miR-51 and let-7 family) or concentrated in a single expression cluster (lin-4 family). Error bars in **a**,**b** are based on random counting statistics. *P* values in **a**,**b** were computed by Fisher's exact test. $*P < 0.05$; $**P < 0.001$.

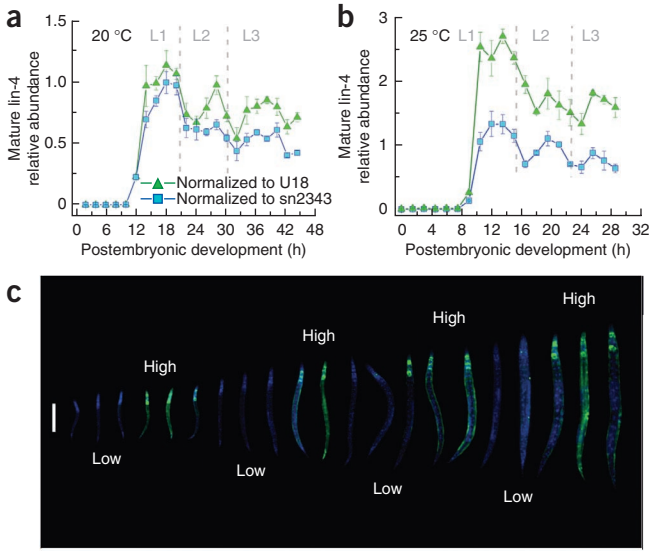


**Figure 4** lin-4 miRNA expression is pulsatile. (**a**,**b**) Mean mature lin-4 levels in staged larvae determined by TaqMan quantitative PCR at 20 °C (**a**) and 25 °C (**b**). Error bars, s.d. ($n > 3$ replicates per condition). Dashed lines separate larval stages. (**c**) *Plin-4*::*GFP* smFISH (green) and DAPI (blue) images of staged larvae are merged and ordered by their body lengths. Scale bar, 100 µm. *Plin-4*::*GFP* contains the promoter of lin-4 fused to the *GFP* gene.

assay for small RNA detection. To our surprise, mature lin-4 expression was also pulsatile, peaking approximately once per larval stage (**Fig. 4a**,**b**). We also investigated the activity of the *lin-4* promoter by measuring the transcript levels of a *lin-4* promoter–*GFP* fusion construct[32] (**Fig. 4c**). The *lin-4* promoter was ubiquitously active in somatic cells but not in the germ line, in agreement with previous reports[32]. Notably, we found that promoter activity of *lin-4* alternated between high and low levels during postembryonic development, with a period of approximately one larval stage (**Fig. 4c**), suggesting that pulsatile mature lin-4 miRNA levels (**Fig. 4a**,**b**) are transcriptionally regulated. Although it is widely accepted that the expression profile of lin-4 miRNA exhibits a gradual 'switch-like' transition[25,33] at the end of L1, our sublarval-stage high-resolution data suggest the existence of intricate dynamics that have not previously been seen.

## Transcript counting by single-molecule *in situ* hybridization confirms the temporal gradient of *lin-14*

Intrigued by this dynamic expression of lin-4 miRNA, we decided to obtain detailed information on the expression dynamics of the canonical lin-4 target and counted individual *lin-14* transcripts in intact worms using a single-molecule fluorescence *in situ* hybridization method (smFISH)[34] (**Fig. 5a**). We obtained high temporal resolution by estimating the postembryonic age of individual worms from body length, defined as the distance between the most anterior nucleus hyp4 and the most posterior nucleus hyp10 along the anteroposterior axis (**Fig. 5b** and **Supplementary Figs. 3–5**). We detected *lin-14* transcripts throughout the body in all previously reported expressing cells[3,11] of wild-type worms during all larval stages from L1 to L4 (**Fig. 5a**). Exceptions were germline and somatic gonad cells, where no *lin-14* transcripts were observed. We determined mRNA concentrations at each developmental time point by normalizing the total transcript count to the volume of the worm[35] (**Supplementary Fig. 6**). We found that the *lin-14* mRNA concentration forms a smooth temporal gradient during postembryonic development (**Fig. 5c**). To test whether these expression dynamics were observed consistently along the anteroposterior axis, we generated anteroposterior mRNA density maps (**Supplementary Fig. 7**). We found that, with the exceptions of the head, tail and germline regions where cell densities are higher, *lin-14* transcripts were equally distributed along the midbody region and were uniformly downregulated during larval development, recapitulating the dynamics observed in the whole worm (**Fig. 5c**).

## Expression of the lin-4 target *lin-14* becomes pulsatile upon loss of lin-4 expression

The pulsatile dynamics of lin-4 miRNA levels are difficult to reconcile with the smooth temporal gradient observed for *lin-14*, which is a direct target of lin-4 (refs. 11,15). To explore why the pulsatile dynamics of lin-4 are not propagated to its target, we measured *lin-14* mRNA concentrations in *lin-4*(*e912*) knockout mutant worms (**Fig. 6a**). During early L1, *lin-14* transcript levels in these mutant worms were identical to those in wild-type worms. However, as larvae entered late L1, *lin-14* concentrations started to exhibit large peaks in the absence of lin-4. The peaks occurred approximately once per larval stage. Our *in situ* results in these mutants faithfully recapitulated our RNA-seq results, suggesting that smFISH reliably detects RNA molecules, even in *C. elegans* larvae with abnormal cuticles (**Supplementary Fig. 8**). We questioned whether this pulsatile dynamic was also present at the level of individual cells and measured *lin-14* mRNA in a group of hypodermal cells, hyp8–hyp11 (five nuclei), at the tail tip that increase in volume but do not divide[36] (**Fig. 6b** and **Supplementary Fig. 9**). In these cells, *lin-14* mRNA dynamics were qualitatively similar to those observed in the entire worm. Next, we generated a map of fold change in *lin-14* transcript numbers and found that its derepression in the absence of lin-4 activity was present globally along the anteroposterior

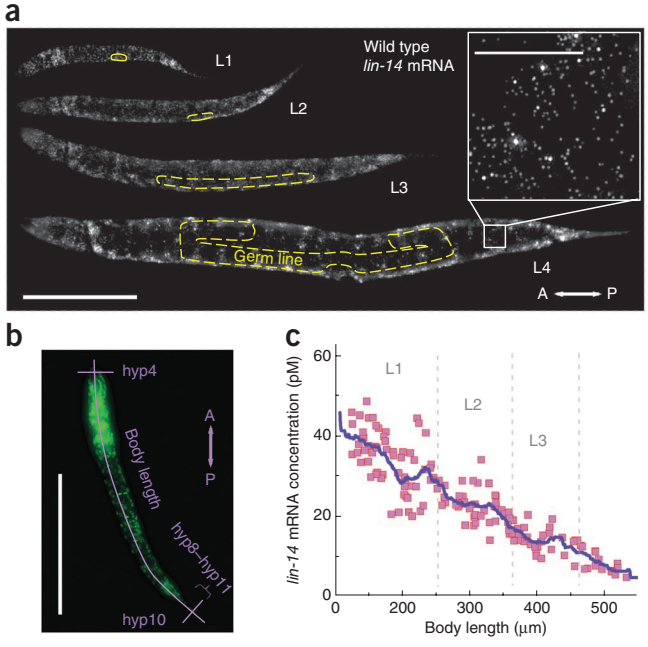


**Figure 5** *lin-14* mRNA is homogeneously expressed in the somatic tissue of worm larvae and exhibits a temporal gradient. (**a**) Maximum *z* projection of *lin-14* smFISH stacked images of staged larvae. Transcripts are visualized as countable fluorescent spots (inset at 8× magnification). Yellow dashed lines outline the germ line and gonad. Scale bars, 100 µm and 12.5 µm (inset). A, anterior; P, posterior. (**b**) Body length determined from DAPI staining (green). (**c**) Overall *lin-14* mRNA concentration of individual animals as a function of body length. The curve indicates a moving average (bin; 36 µm). Dashed lines separate larval stages.

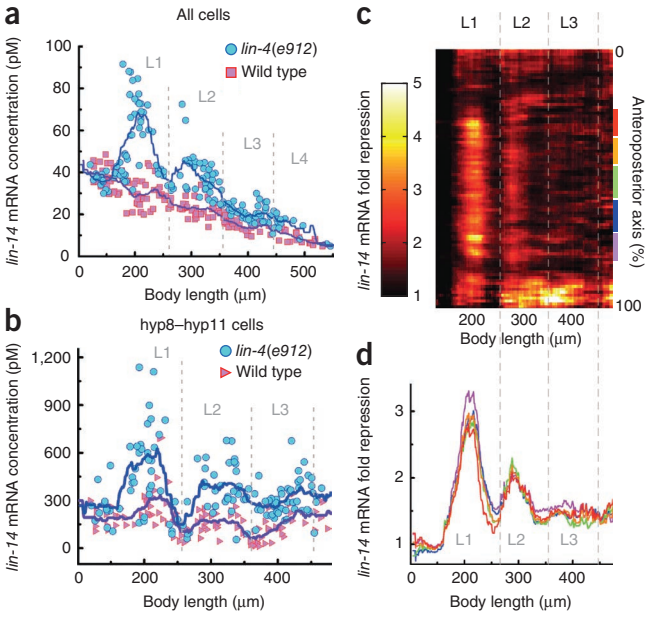


**Figure 6** *lin-14* mRNA levels exhibit pulsatile dynamics in the absence of lin-4 negative regulation. (**a**,**b**) *lin-14* mRNA concentration dynamics of individual *lin-4*(*e912*) mutants as a function of body length. Shown are the overall concentration (**a**) and the local concentration in hyp8–hyp11 (**b**). Curves in **a**,**b** indicate moving averages (bin size, 36 μm), and dashed lines separate larval stages. (**c**) Anteroposterior map of fold repression of *lin-14* mRNA in wild-type worms compared to in *lin-4*(*e912*) mutants. Anteroposterior axis percentage indicates relative position along the anteroposterior axis (0%, head; 100%, tail). The height of each bin is 1%, and a moving average (bin size, 36 μm) is applied in the *x* direction. (**d**) Fold repression of *lin-14* mRNA in the midbody. Each curve represents a trajectory along the *x* axis of the heatmap in **c**, where its corresponding color is defined.

axis (**Fig. 6c**). Each colored bin indicates the fold change in *lin-14* transcript numbers in *lin-4*(*912*) worms compared to wild-type worms at a given location along the anteroposterior body axis and at a given postembryonic age. Recurring vertical bands in this map reflect the fact that the timing of pulses in *lin-14* transcript levels is synchronized in every segment of the body along the anteroposterior axis. We examined the midbody region of the worms, which uniformly comprises hypodermal, intestinal and muscle cells, and indeed found a transient ~3-fold repression of *lin-14* transcript levels in wild-type worms compared to *lin-4*(*e912*) worms during the L1 and L2 stages (**Fig. 6d** and **Supplementary Fig. 8**). The strength of transient repression was further reduced during the L3 stage, reaching a steady ~1.5-fold repression. Because *lin-4*(*e912*) worms exhibit reiterating L1 fates (hatch → L1 → L1 → L1 →)[10,13], it is possible that pulsatile changes in *lin-14* transcript levels are merely a repetition of L1 fate-specific pulses. However, we observed similar dynamics for *lin-14* transcript levels in *lin-4*(*e912*); *lin-14*(*n179ts*) worms with a 'precocious' phenotype, in which the L1-specific larval program is skipped (hatch → L2 → L3 → L4 →)[10], suggesting that pulses in *lin-14* transcript levels are not specific to L1 (**Supplementary Fig. 10**).

### Dampening of fluctuations in *lin-14* transcript levels is directly mediated by lin-4 target sites in its 3′ UTR

To examine whether the pulsatile *lin-14* transcript levels observed in *lin-4*(*e912*) worms were caused by the absence of direct interaction between lin-4 and the *lin-14* 3′ UTR, we counted *lin-14* transcripts in *lin-14*(*n355gf*) worms (**Supplementary Fig. 11**), which lack all of seven putative lin-4 complementary elements (LCEs) owing to

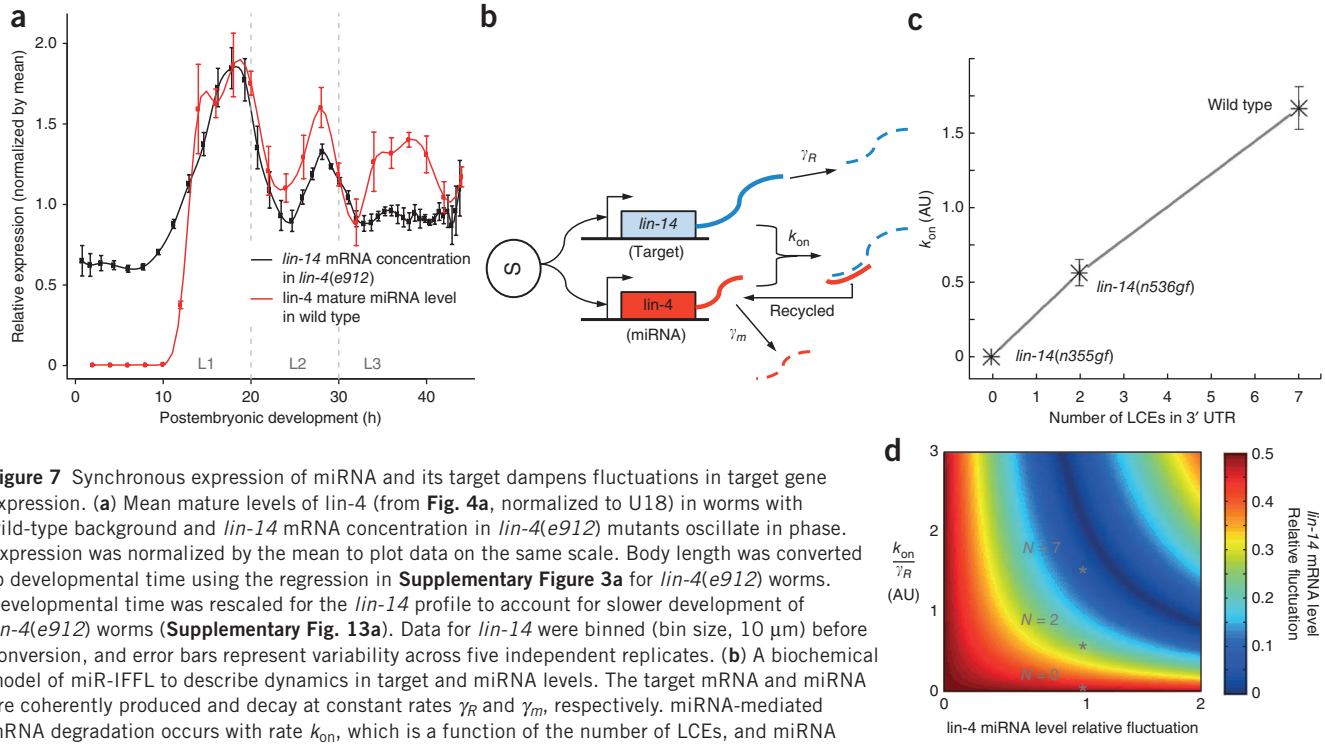


**Figure 7** Synchronous expression of miRNA and its target dampens fluctuations in target gene expression. (**a**) Mean mature levels of lin-4 (from **Fig. 4a**, normalized to U18) in worms with wild-type background and *lin-14* mRNA concentration in *lin-4*(*e912*) mutants oscillate in phase. Expression was normalized by the mean to plot data on the same scale. Body length was converted to developmental time using the regression in **Supplementary Figure 3a** for *lin-4*(*e912*) worms. Developmental time was rescaled for the *lin-14* profile to account for slower development of *lin-4*(*e912*) worms (**Supplementary Fig. 13a**). Data for *lin-14* were binned (bin size, 10 μm) before conversion, and error bars represent variability across five independent replicates. (**b**) A biochemical model of miR-IFFL to describe dynamics in target and miRNA levels. The target mRNA and miRNA are coherently produced and decay at constant rates $\gamma_R$ and $\gamma_m$, respectively. miRNA-mediated mRNA degradation occurs with rate $k_{on}$, which is a function of the number of LCEs, and miRNA is recycled. The capital S indicates an alternating source of input. (**c**) $k_{on}$ fit values for *lin-14* alleles with different numbers of LCEs. Error bars correspond to 95% confidence intervals. AU, arbitrary units. (**d**) miR-IFFL performance landscape. Damping is efficient when miRNA is expressed synchronously with its target (lin-4 miRNA relative fluctuation >0) with an optimal value of $k_{on}$ (dark-blue valley). Asterisks indicate *lin-14* alleles with different numbers of LCEs (*N*).

genomic rearrangements[37,38]. We found that *lin-14* mRNA levels also exhibited pulsatile dynamics in *lin-14*(*n355gf*) worms similar to those observed in *lin-4*(*e912*) worms (**Fig. 6a**,**b**). In addition, we measured transcripts in *lin-14*(*n536gf*) worms, which carry only two LCEs owing to a deletion in the 3′ UTR[37,38], and observed a similarly spaced train of peaks with reduced amplitudes (**Supplementary Fig. 12**). These data suggest that the pulsatile *lin-14* expression observed in mutant worms is attributed to the loss of a direct interaction between lin-4 and the *lin-14* 3′ UTR.

### An incoherent feed-forward loop mediated by lin-4 can efficiently insulate *lin-14* from pulsatile expression dynamics

To understand how the miRNA lin-4 can eliminate pulses in the transcript levels of its targets, we compared the timing of *lin-4* and *lin-14* peak expression. First, we tested for a difference in developmental timing in wild-type and *lin-4*(*e912*) worms by comparing temporal expression profiles in the two strains across all genes, measuring a small delay for *lin-4*(*e912*) worms. After conversion of body length into time (**Supplementary Fig. 3a**) and rescaling of developmental time in *lin-4*(*e912*) worms by a factor of 0.85 to account for developmental delay (**Supplementary Fig. 13a**), we could directly compare the expression of *lin-4* in wild-type worms and *lin-14* in *lin-4*(*e912*) worms as a function of developmental time. We found that the peaks corresponding to mature lin-4 miRNA levels (as quantified from **Fig. 4a**) coincided with the peaks of *lin-14* transcript levels in *lin-4*(*e912*) worms (**Fig. 7a**). Given that the spatial expression patterns of *lin-4* and *lin-14* are similar and that lin-4 acts cell autonomously[39], these results suggest that *lin-4* and its target *lin-14* are synchronously expressed by a pulsatile cue in individual cells.

Taking these data together, we suggest that the pulsatile transcript levels of *lin-14* are effectively dampened by synchronized pulsatile expression of their negative regulator *lin-4* in wild-type worms. The gene network motif composed of lin-4 miRNA and its target *lin-14* can be classified as an 'incoherent feed-forward loop' (IFFL)[18] (**Fig. 7b**). To quantitatively understand how a miRNA-mediated IFFL (miR-IFFL) motif can efficiently dampen oscillations of target mRNAs, we built a mathematical model to characterize the dynamics of target gene levels in the presence of miRNA activity (**Fig. 7b** and **Supplementary Note**). We assumed a synchronous periodic production of the target mRNA and miRNA, with decays described by first-order constant rates $\gamma_R$ and $\gamma_m$, respectively. We also assumed irreversible second-order kinetics for miRNA-mediated target transcript degradation, with a rate constant $k_{on}$. The rate $k_{on}$ depends on the strength of the miRNA-target interaction, which is proportional to the number of miRNA complementary elements $N$ in the target transcript (thus, $k_{on}(N = 0) = 0$ in both the *lin-4*(*e912*) and *lin-14*(*n355gf*) strains). We assumed steady-state dynamics and fitted this model to the experimental data (**Supplementary Fig. 13b**–**h**). This simple model described the experimental data well, and, reassuringly, we found a linear correlation between $k_{on}$ and the number $N$ of LCEs in the *lin-14* 3′ UTR (**Fig. 7c**).

To test the role of synchronous expression of the miRNA and its target, we explored the parameter space of the miR-IFFL as an insulator of pulsatile input signals using the model described above. We found that relative fluctuations in *lin-14* mRNA levels were minimized only when relative fluctuations in miRNA levels were nonzero and were optimally balanced with the strength of miRNA-target interaction constant $k_{on}$ (**Fig. 7d**, dark-blue valley and **Supplementary Fig. 14**).

## DISCUSSION

Whereas, previously, only a handful of genes were shown to have expression peaking during each larval stage[5,40,41], we found that approximately 2,000 genes exhibit oscillations in temporal expression that are synchronized with the molting cycle. Most other genes are either expressed at a constant level, become upregulated upon gametogenesis in the germ line or display a temporal gradient, akin to those of well-studied heterochronic cell fate regulators. Two modes of timekeeping are apparently at work during nematode larval development: temporal gradients of cell-fate regulators control the transition between subsequent larval stage–specific programs, and periodically expressed genes control progression of the molting cycle. Although the heterochronic pathway and the molting cycle are likely to be linked at the molecular level to coordinate larval transitions with interlarval molts, the temporal gradients of heterochronic cell fate regulators need to be efficiently insulated from temporal fluctuations. Our cluster analysis provides a clue that miRNAs are more generally involved in the maintenance of oscillatory and graded expression patterns. We followed up by quantitatively examining the expression dynamics of the canonical miRNA-target pair lin-4 and *lin-14* and show that miR-IFFLs actively insulate temporal gradient genes from these global oscillations. It has previously been demonstrated that an IFFL can generate a gene expression pulse when the response time of its negative component is slow[18]. Our findings suggest that an IFFL can instead eliminate a gene expression pulse when it is mediated by negative components with fast response times[42], such as miRNAs that are short and do not require translation to be functional. We suggest that a miR-IFFL could be a simple but powerful design motif that dynamic gene regulatory networks of multicellular organisms can adopt to insulate genes from highly dynamic but undesired inputs. Given its prevalence throughout different species[43], this design motif might serve similar function in other species.

## METHODS

Methods and any associated references are available in the online version of the paper.

**Accession codes.** Transcript sequencing data have been deposited under GenBank Gene Expression Omnibus (GEO) accession GSE49043.

*Note: Any Supplementary Information and Source Data files are available in the online version of the paper.*


### ACKNOWLEDGMENTS

We thank V. Ambros, H.R. Horvitz, G. Ruvkun and J. Gore for helpful discussions and advice. We thank S. Itzkovitz, J.P. Junker, G. Neuert, J. van Zon, A. Sahay and C. Engert for a critical reading of the manuscript. We thank the Massachusetts Institute of Technology (MIT) BioMicro Center for Illumina sample preparation and sequencing experiments. We also thank the Biopolymers & Proteomics Core Facility of the MIT Koch Institute for Integrative Cancer Research for probe purification. Several nematode strains used in this work were provided by H.R. Horvitz (Massachusetts Institute of Technology) and A. Fire (Stanford University) and the *Caenorhabditis* Genetics Center, which is funded by the US National Institutes of Health (NIH) and National Center for Research Resources (NCRR). This work was supported by the US NIH/National Cancer Institute Physical Sciences Oncology Center at MIT (U54CA143874), a US NIH Pioneer award (8 DP1 CA174420-05), a European Research Council Advanced grant (ERC-AdG 294325-GeneNoiseControl) and a Green Cross Corp. (Republic of Korea) Mogam Science Scholarship.


### AUTHOR CONTRIBUTIONS

D.h.K. and A.v.O. conceived the project and designed the experiments. D.h.K. performed the experiments. D.h.K., D.G. and A.v.O. analyzed the data and wrote the manuscript.

### COMETING FINANCIAL INTERESTS

The authors declare no competing financial interests.

1. Raj, A. & van Oudenaarden, A. Nature, nurture, or chance: stochastic gene expression and its consequences. *Cell* **135**, 216–226 (2008).
2. Rougvie, A.E. Intrinsic and extrinsic regulators of developmental timing: from miRNAs to nutritional cues. *Development* **132**, 3787–3798 (2005).
3. Ruvkun, G. & Giusto, J. The *Caenorhabditis elegans* heterochronic gene *lin-14* encodes a nuclear protein that forms a temporal developmental switch. *Nature* **338**, 313–319 (1989).
4. Johnstone, I.L. & Barry, J.D. Temporal reiteration of a precise gene expression pattern during nematode development. *EMBO J.* **15**, 3633–3639 (1996).
5. Gissendanner, C.R., Crossgrove, K., Kraus, K.A., Maina, C.V. & Sluder, A.E. Expression and function of conserved nuclear receptor genes in *Caenorhabditis elegans*. *Dev. Biol.* **266**, 399–416 (2004).
6. Raizen, D.M. *et al.* Lethargus is a *Caenorhabditis elegans* sleep-like state. *Nature* **451**, 569–572 (2008).
7. Page, A.P. & Johnstone, I.L. The cuticle. *WormBook* http://www.wormbook.org/ (2007). doi:10.1895/wormbook.1.138.1.
8. Altun, Z.F. & Hall, D.H. Introduction. *WormAtlas* http://www.wormatlas.org (2009).
9. Hubbard, E.J.A. & Grenstein, D. Introduction to the germ line. *WormBook* http://www.wormbook.org/ (2005). doi:10.1895/wormbook.1.18.1.
10. Ambros, V. & Horvitz, H.R. The *lin-14* locus of *Caenorhabditis elegans* controls the time of expression of specific postembryonic developmental events. *Genes Dev.* **1**, 398–414 (1987).
11. Moss, E.G., Lee, R.C. & Ambros, V. The cold shock domain protein LIN-28 controls developmental timing in *C. elegans* and is regulated by the *lin-4* RNA. *Cell* **88**, 637–646 (1997).
12. Slack, F.J. *et al.* The *lin-41* RBCC gene acts in the *C. elegans* heterochronic pathway between the *let-7* regulatory RNA and the LIN-29 transcription factor. *Mol. Cell* **5**, 659–669 (2000).
13. Ambros, V. & Horvitz, H. Heterochronic mutants of the nematode *Caenorhabditis elegans*. *Science* **226**, 409–416 (1984).
14. Ambros, V. A hierarchy of regulatory genes controls a larva-to-adult developmental switch in *C. elegans*. *Cell* **57**, 49–57 (1989).
15. Lee, R.C., Feinbaum, R.L. & Ambros, V. The *C. elegans* heterochronic gene *lin-4* encodes small RNAs with antisense complementarity to *lin-14*. *Cell* **75**, 843–854 (1993).
16. Bartel, D.P. MicroRNAs: target recognition and regulatory functions. *Cell* **136**, 215–233 (2009).
17. Reinhart, B.J. & Ruvkun, G. Isoform-specific mutations in the *Caenorhabditis elegans* heterochronic gene *lin-14* affect stage-specific patterning. *Genetics* **157**, 199–209 (2001).
18. Alon, U. Network motifs: theory and experimental approaches. *Nat. Rev. Genet.* **8**, 450–461 (2007).
19. Gerstein, M.B. *et al.* Integrative analysis of the *Caenorhabditis elegans* genome by the modENCODE project. *Science* **330**, 1775–1787 (2010).
20. Mortazavi, A., Williams, B.A., Mccue, K., Schaeffer, L. & Wold, B. Mapping and quantifying mammalian transcriptomes by RNA-Seq. *Nat. Methods* **5**, 1–8 (2008).
21. Sönnichsen, B. *et al.* Full-genome RNAi profiling of early embryogenesis in *Caenorhabditis elegans*. *Nature* **434**, 462–469 (2005).
22. Lewis, B.P., Burge, C.B. & Bartel, D.P. Conserved seed pairing, often flanked by adenosines, indicates that thousands of human genes are microRNA targets. *Cell* **120**, 15–20 (2005).
23. Selbach, M. *et al.* Widespread changes in protein synthesis induced by microRNAs. *Nature* **455**, 58–63 (2008).
24. Baek, D. *et al.* The impact of microRNAs on protein output. *Nature* **455**, 64–71 (2008).
25. Bagga, S. *et al.* Regulation by *let-7* and *lin-4* miRNAs results in target mRNA degradation. *Cell* **122**, 553–563 (2005).
26. Lim, L.P. *et al.* Microarray analysis shows that some microRNAs downregulate large numbers of target mRNAs. *Nature* **433**, 769–773 (2005).
27. Dreszer, T.R. *et al.* The UCSC Genome Browser database: extensions and updates 2011. *Nucleic Acids Res.* **40**, D918–D923 (2012).
28. Zhang, X., Zabinsky, R., Teng, Y., Cui, M. & Han, M. microRNAs play critical roles in the survival and recovery of *Caenorhabditis elegans* from starvation-induced L1 diapause. *Proc. Natl. Acad. Sci. USA* **108**, 17997–18002 (2011).
29. de Lencastre, A. *et al.* MicroRNAs both promote and antagonize longevity in *C. elegans*. *Curr. Biol.* **20**, 2159–2168 (2010).
30. Boulias, K. & Horvitz, H.R. The *C. elegans* microRNA *mir-71* acts in neurons to promote germline-mediated longevity through regulation of DAF-16/FOXO. *Cell Metab.* **15**, 439–450 (2012).
31. Alvarez-Saavedra, E. & Horvitz, H.R. Many families of *C. elegans* microRNAs are not essential for development or viability. *Curr. Biol.* **20**, 367–373 (2010).
32. Martinez, N.J. *et al.* Genome-scale spatiotemporal analysis of *Caenorhabditis elegans* microRNA promoter activity. *Genome Res.* **18**, 2005–2015 (2008).
33. Feinbaum, R. & Ambros, V. The timing of *lin-4* RNA accumulation controls the timing of postembryonic developmental events in *Caenorhabditis elegans*. *Dev. Biol.* **210**, 87–95 (1999).
34. Raj, A., Bogaard, P.V.D., Rifkin, S.A., Oudenaarden, A.V. & Tyagi, S. Imaging individual mRNA molecules using multiple singly labeled probes. *Nat. Methods* **5**, 877–879 (2008).
35. Knight, C.G., Patel, M.N., Azevedo, R.B.R. & Leroi, A.M. A novel mode of ecdysozoan growth in *Caenorhabditis elegans*. *Evol. Dev.* **4**, 16–27 (2002).
36. Sulston, J.E. & Horvitz, H.R. Post-embryonic cell lineages of the nematode, *Caenorhabditis elegans*. *Dev. Biol.* **56**, 110–156 (1977).
37. Ruvkun, G. *et al.* Molecular genetics of the *Caenorhabditis elegans* heterochronic gene *lin-14*. *Genetics* **121**, 501–516 (1989).
38. Wightman, B., Ha, I. & Ruvkun, G. Posttranscriptional regulation of the heterochronic gene *lin-14* by *lin-4* mediates temporal pattern formation in *C. elegans*. *Cell* **75**, 855–862 (1993).
39. Zhang, H. & Fire, A.Z. Cell autonomous specification of temporal identity by *Caenorhabditis elegans* microRNA *lin-4*. *Dev. Biol.* **344**, 603–610 (2010).
40. Jeon, M. Similarity of the *C. elegans* developmental timing protein LIN-42 to circadian rhythm proteins. *Science* **286**, 1141–1146 (1999).
41. Frand, A.R., Russel, S. & Ruvkun, G. Functional genomic analysis of *C. elegans* molting. *PLoS Biol.* **3**, e312 (2005).
42. Basu, S., Mehreja, R., Thiberge, S., Chen, M.-T. & Weiss, R. Spatiotemporal control of gene expression with pulse-generating networks. *Proc. Natl. Acad. Sci. USA* **101**, 6355–6360 (2004).
43. Tsang, J., Zhu, J. & van Oudenaarden, A. MicroRNA-mediated feedback and feedforward loops are recurrent network motifs in mammals. *Mol. Cell* **26**, 753–767 (2007).

## ONLINE METHODS

**Strains.** *C. elegans* strains used in this study were N2 (wild type), MT873 (*lin-4*(*e912*)*II*), MT355 (*lin-14*(*n355gf*)*X*), MT536 (*lin-14*(*n536gf*)*X*), VT1072 (*unc-119*(*ed3*)*III*; *maIs134*[*unc-119*(+) + *Plin-4*::*GFP*]), MT723 (*lin-4*(*e912*)*II*; *lin-14*(*n179ts*)*X*) and PD7190 (*lin-4*(*e912*)/*mC6 II*; *pha-1*(*e2123ts*) *III*; *rde-1*(*ne300*) *V*; *pHZ081* [*pcol-10*::*lin-4*::*let-858_3′ UTR*]; *pC1* [*pha-1*(+)]).

**Synchronization and RNA extraction.** Wild-type (N2) and mutant nematodes were synchronized by hypochlorite treatment. L1-arrested worms in starvation medium were spotted onto NGM (Nematode Growth Media) plates with food (OP50 *Escherichia coli* strain) and cultured at 20 °C unless otherwise stated. Total RNA was isolated from synchronized larval populations using TRIzol (Invitrogen). Each sample underwent three rounds of freeze-thaw cycles for enhanced efficiency.

**Sequencing of polyadenylated RNA.** Poly(A)$^+$ RNA libraries were prepared from total RNA. Reads were aligned with Burrows-Wheeler Aligner (BWA)[44] using default parameters to modENCODE integrated transcript models on the basis of WormBase Release ws190 (ref. 19). Reads were aggregated across isoforms, and expression per gene locus was calculated in reads per million mapped reads (RPM). Whenever expression was measured in RPKM, the length of merged isoforms was used for normalization[20].

**Inference of expression clusters.** The expression profile of each gene was normalized by the sum of expression values across all time points and was log transformed. Normalized expression profiles were topologically ordered into a two-dimensional discrete map with $20 \times 20$ grid points using a self-organizing map[45], implemented in R (SOM package). The self-organizing map was then subjected to robust *k*-means clustering with 100 bootstraps, implemented in R (fpc package), using $k = 8$. The value of $k$ was optimized to obtain the best coverage of the self-organizing map. Clusters with Jaccard similarity <0.6 across bootstrap runs were not considered robust and were discarded.

**Identification of human orthologs.** One-to-one human orthologs of *C. elegans* genes were identified by running BLASTP[46] on translated protein sequences. Only significant ($E < 1 \times 10^{-10}$) reciprocal best hits were retained.

**GO term analysis.** GO term analysis was performed in R using the GOstats package[47]. Over-represented GO terms for each expression cluster were computed against the background of all genes falling into one of the robust clusters.

**smFISH.** Probe design and hybridization for smFISH in *C. elegans* larvae was performed as previously described[34]. We used M9 to wash larvae off of plates. Larvae were additionally washed twice to empty the gut filled with bacteria and were fixed in 4% formaldehyde in 1× PBS for 45 min. Fixed larvae were permeabilized in 70% ethanol overnight. All probes were coupled to either Cy5 (GE Amersham) or Alexa Fluor 594 (Invitrogen), which gave us a high signal-to-background ratio in all larval stages. Hybridized larvae were imaged using a Nikon Ti-E inverted fluorescence microscope equipped with a 100× oil-immersion objective and a Photometrics Pixis 1024 CCD camera using MetaMorph software (Molecular Devices) and appropriate optical filters for Cy5, Alexa Fluor 594 and DAPI. Data analyses and model simulations were carried out semiautomatically with the aid of custom software written in MATLAB (Mathworks).

**miRNA TaqMan PCR assays.** TaqMan PCR assays for lin-4 miRNA quantification were performed following the instructions from the manufacturer (Applied Biosystems) using a Light Cycler 480 II Real-Time PCR machine (Roche). We used sn2343 and U18 as controls for normalization.


44. Li, H. & Durbin, R. Fast and accurate long-read alignment with Burrows-Wheeler transform. *Bioinformatics* **26**, 589–595 (2010).
45. Kohonen, T. Self-organized formation of topologically correct feature maps. *Biol. Cybern.* **43**, 59–69 (1982).
46. Altschul, S.F., Gish, W., Miller, W., Myers, E.W. & Lipman, D.J. Basic local alignment search tool. *J. Mol. Biol.* **215**, 403–410 (1990).
47. Falcon, S. & Gentleman, R. Using GOstats to test gene lists for GO term association. *Bioinformatics* **23**, 257–258 (2007).